Dynamic Trap States of Dual-Spin Spacecraft

M. P. SCHER* AND R. L. FARRENKOPF†
TRW Systems Group, Redondo Beach, Calif.

Two trap states are identified for spacecraft having asymmetric or unbalanced rotors. The first is a minimum energy state to which the spacecraft settles when the despin motor is deactivated. The second, encountered while despinning the platform, is characterized by a stalling of the despin process and a violent increase in nutation. Analysis demonstrates that, in both trap states, the spacecraft possesses two modes of attitude motion, each with a distinct frequency. Excitation by the motor at an appropriate natural frequency can lead to escape from either trap, even when the motor torque is insufficient to permit direct despin.

Introduction

New Problem Area

IMPORTANT dynamical problems are masked by assumptions often invoked in the analysis of attitude motions of dual-spin spacecraft. Specifically, it is commonly assumed that: 1) the spacecraft's rotor is a statically and dynamically balanced symmetric body, perhaps containing a damper; 2) the rotor either spins at a constant angular rate relative to the platform or possesses a constant inertial spin rate about its symmetry axis; and 3) the platform, which may be asymmetric and unbalanced, is in or near a despun condition.

While the attendant analytical simplifications often warrant consideration of balanced symmetrical rotors, mass property imperfections can introduce some undesirable dynamic effects. These imperfections have a major impact once the despin motor has been deactivated, allowing bearing friction to slow the relative motion until both bodies rotate as a unit and settle to a state of minimum energy. Reactivation of the motor at this point may prove futile because restraint torques, arising in part from the rotor imperfections, can lock the platform to the rotor. The spacecraft is then said to be in a minimum energy trap state. Even if this lock can be broken, the process of despinning the platform might be interrupted by the onset of violent nutation. In this latter trap, nutation grows ever greater as the motor adds energy to the system while the despin process stalls.

Both of these traps can be demonstrated by a dynamic model consisting of two rigid bodies having a single degree of relative rotational freedom controlled by a motor. One rigid body represents the rotor and is balanced, but asymmetric. The second body, or platform, is statically balanced and symmetric, but dynamically unbalanced. Neither dampers nor external torques need be considered. A salient feature of this model, and of a dual-spin spacecraft in general, is that its unforced attitude motion is a combination of two modes having distinct frequencies. One of these modes resembles nutation, while the second has a lower, and heretofore undiscovered, frequency. Excitation of the system by the despin motor at the latter frequency provides a means for escape from either trap.

Previous Dual-Spin Investigations

Earlier papers focus on unusual states of motion which dual-spin spacecraft can attain. One emphasizes the effects of energy dissipators on one or both bodies,[1] while others consider the influence of gravitational torques.[2,3] Yet others examine trap states dependent on the peculiarities of nutation dampers.[4-7] Numerous papers treat stability of the nominal motion in which the platform is rotationally at rest (e.g., see bibliographies in Refs. 1 and 6). All of these restrict consideration to spacecraft with balanced symmetric rotors and constant rotor rates. One or the other of these restrictions has been relaxed, but never both simultaneously. Platform pointing errors induced by rotor dynamic imbalance have been assessed,[8] and techniques for their attenuation demonstrated.[9,10] The dynamics of rotor spin-up have also been considered, but only with a symmetric rotor.[11]

The most relevant area of previous research involves recovery of prolate-shaped spinning spacecraft from flat-spin conditions.[12] The minimum energy trap discussed herein contains aspects common to the flat-spin problem, but an oblate-shaped spacecraft is considered here in order to demonstrate the second and more unique trap as well.

Model

A dual-spin system exhibiting both types of trap states is shown in Fig. 1. The system is comprised of a rigid rotor A and a rigid platform B whose respective mass centers, A^* and B^*, lie on the bearing axis X_1 and are separated by a distance r. Fixed in body A are two additional axes, X_2 and X_3, perpendicular both to each other and to X_1 and intersecting at A^*. Mutually perpendicular axes, Y_2 and Y_3, are fixed in B, also normal to X_1, and intersect at B^*. The orientation of B relative to A about X_1 is specified by the angle α between Y_3 and the X_1-X_3 plane. Increases in α correspond to right-handed rotations of B relative to A about X_1.

Bodies A and B have masses m_A and m_B, respectively. The bodies' individual centroidal inertia tensors, $[A]$ and $[B]$, referred to their respective axis sets (i.e., X_1, X_2, X_3 and X_1, Y_2, Y_3) are of the following form:

$$[A]=\begin{bmatrix} A_1 & 0 & 0 \\ 0 & A_2 & 0 \\ 0 & 0 & A_3 \end{bmatrix} \qquad [B]=\begin{bmatrix} B_1 & 0 & P \\ 0 & B_3 & 0 \\ P & 0 & B_3 \end{bmatrix} \tag{1}$$

Here both bodies are statically balanced since their mass centers lie on the bearing axis. Body A is dynamically balanced since

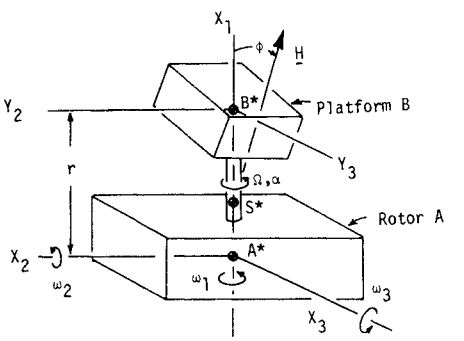

Fig. 1 Model with asymmetric rotor and platform dynamic imbalance.

Received August 17, 1973; presented as Paper 73-908 at the AIAA Guidance and Control Conference, Key Biscayne, Fla., August 20–22, 1973; revision received June 3, 1974.
Index category: Spacecraft Attitude Dynamics and Control.
* Section Head, Dynamics Department. Member AIAA.
† Senior Staff Engineer, Control and Sensor Systems Laboratory.

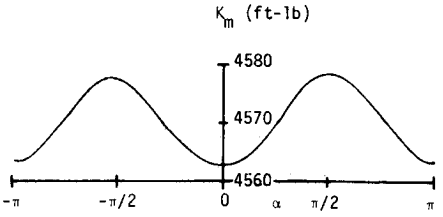

Fig. 2 Minimum kinetic energy as a function of α.

the bearing axis is one of its principal axes. However, A is asymmetric since A_2 and A_3 are assumed unequal. Body B is symmetric about the bearing axis, as evidenced by the double entry of B_3 in its inertia tensor. However, B is dynamically unbalanced since the bearing axis is not a principal axis of inertia. Specifically, B has a product of inertia P in the X_1–Y_3 plane.

Equations of motion for the system are presented (without derivation) in terms of α, its time derivative Ω, and of $\omega_1, \omega_2, \omega_3$, the three components of the inertial angular velocity of A referred to X_1, X_2, X_3. These equations are cast in matrix form as

$$[E][\dot{Z}] = [F] \tag{2}$$

where $[E]$ is a 5×5 symmetric matrix and both $[Z]$ and $[F]$ are 5×1. Here‡

$$[Z]^T = [\omega_1, \omega_2, \omega_3, \Omega, \alpha] \tag{3}$$

Elements of $[E]$ and $[F]$ are readily specified after defining

$$\begin{aligned} I &= A_1 + B_1 \\ J &= A_2 + B_3 + r^2 m_A m_B/(m_A+m_B) \\ K &= A_3 + B_3 + r^2 m_A m_B/(m_A+m_B) \end{aligned} \tag{4}$$

Here I, J, K are the moments of inertia of the entire spacecraft about lines parallel to X_1, X_2, X_3 and passing through the spacecraft mass center S^*. In terms of these three quantities, together with P and the platform's moment of inertia B_1 about X_1, the nonzero elements of $[E]$ and $[F]$ are

$$\begin{aligned} &E_{11} = I \quad E_{22} = J \quad E_{33} = K \\ &E_{44} = E_{14} = E_{41} = B_1 \quad E_{55} = 1 \\ &E_{12} = E_{21} = E_{24} = E_{42} = -P\sin\alpha \\ &E_{13} = E_{31} = E_{34} = E_{43} = P\cos\alpha \end{aligned} \tag{5}$$

$$\begin{aligned} F_1 &= (J-K)\omega_2\omega_3 - P\omega_1(\omega_2\cos\alpha + \omega_3\sin\alpha) \\ F_2 &= (K-I)\omega_1\omega_3 + P[(\omega_1+\Omega)^2 - \omega_3{}^2]\cos\alpha + \\ &\qquad P\omega_2\omega_3\sin\alpha - B_1\Omega\omega_3 \\ F_3 &= (I-J)\omega_1\omega_2 + P[(\omega_1+\Omega)^2 - \omega_2{}^2]\sin\alpha + \\ &\qquad P\omega_2\omega_3\cos\alpha + B_1\Omega\omega_2 \\ F_4 &= T_1 - P\omega_1(\omega_2\cos\alpha + \omega_3\sin\alpha) \\ F_5 &= \Omega \end{aligned} \tag{6}$$

where T_1 is the sum of motor and friction torques applied to B about X_1.

Of future interest are some additional quantities conveniently introduced at this point. The first is the 3×3 inertia tensor $[I]$ of the entire system about S^*, referred to X_1, X_2, X_3. Elements I_{ij} are given by

$$I_{ij} = E_{ij} \qquad i,j = 1,2,3 \tag{7}$$

Next, the rotational kinetic energy K_e of the system about S^* is given by

$$K_e = \sum_{i=1}^{4}\sum_{j=1}^{4} E_{ij}Z_iZ_j/2 \tag{8}$$

Finally, the nutation angle ϕ between X_1 and the system's centroidal angular momentum vector $\mathbf{H}$ is defined as

$$\phi = \tan^{-1}[(h_2{}^2+h_3{}^2)/h_1{}^2]^{1/2} \tag{9}$$

‡ A superscript T denotes the matrix transpose.

where h_i, the component of $\mathbf{H}$ along X_i, is given by

$$h_i = \sum_{j=1}^{4} E_{ij}Z_j \qquad i = 1,2,3 \tag{10}$$

Since no external torques are imposed, $\mathbf{H}$ must remain fixed both in magnitude and inertial orientation.

Portions of the sequel rely on simulation results generated using the following values:

$$\begin{aligned} I &= 350 \text{ slg-ft}^2 & J &= 250 \text{ slg-ft}^2 \\ K &= 275 \text{ slg-ft}^2 & B_1 &= 50 \text{ slg-ft}^2 \\ P &= 20 \text{ slg-ft}^2 & |\mathbf{H}| &= 1800 \text{ ft-lb-sec} \\ |T_1| &= \begin{cases} 1.25 \text{ ft-lb (motor net torque)} \\ 0.25 \text{ ft-lb (friction alone)} \end{cases} \end{aligned} \tag{11}$$

These parameters correspond roughly to a typical 1000 lb spacecraft having a 9-ft-diam rotor spinning nominally at 6 rad/sec. Equations (1–11) provide the analytical basis for discussion of both traps.

Minimum Energy Trap

Heuristic Description

It is well-known that a damped spinning system will seek an energy state that is a local minimum compatible with the system's angular momentum. Application of this principle to a single quasi-rigid body reveals that the minimum energy state is one of spin about the body's centroidal principal axis of maximum inertia.[13] This result can be extended to the present model if only viscous friction acts about X_1 in which case Ω must eventually vanish since finite energy cannot be dissipated indefinitely. Thus ultimately B stops relative to A and the combined system, behaving as a quasi-rigid body, settles to its minimum energy state. The kinetic energy of the system in this state can be determined as a function of α by first computing the maximum centroidal principal moment of inertia of the system, Λ, as the largest eigenvalue of $[I]$ given by Eqs. (5) and (7), i.e., by solving for the maximum positive root of the polynominal

$$\lambda^3 + a_2\lambda^2 + a_1\lambda + a_0 = 0 \tag{12}$$

where

$$\begin{aligned} a_0 &= P^2(J\cos^2\alpha + K\sin^2\alpha) - IJK \\ a_1 &= IJ + IK + KJ - P^2 \\ a_2 &= -(I+J+K) \end{aligned} \tag{13}$$

Noting that the spin rate ω of the system in this state is $\omega(\alpha) = |\mathbf{H}|/\Lambda(\alpha)$, the corresponding minimum kinetic energy K_m can be obtained as

$$K_m(\alpha) = \Lambda\omega^2/2 = |\mathbf{H}|^2/2\Lambda(\alpha) \tag{14}$$

For the values in Eqs. (11), $K_m(\alpha)$ is shown in Fig. 2. Applying the aforementioned minimum energy principle, Fig. 2 now identifies $\alpha = n\pi$ (where n is any integer) as those constant relative angles to which α will converge.

These minimum energy traps have serious implications if the motor torque is insufficient to produce platform despin. A conservative estimate of the required motor torque is the maximum torque needed to hold B fixed relative to A in the minimum energy state corresponding to any possible value of α. This restraint torque T_r as a function of α can be shown to be given by $T_r = dK_m/d\alpha = (dK_m/d\Lambda)[d\Lambda/d\alpha]$. The derivative in brackets may be evaluated implicitly from Eq. (12). Then

$$T_r = 0.5\,|\mathbf{H}/\Lambda|^2 \left\{\frac{\Lambda^2(da_2/d\alpha) + \Lambda(da_1/d\alpha) + (da_0/d\alpha)}{3\Lambda^2 + 2a_2\Lambda + a_1}\right\} \tag{15}$$

For the system of Eqs. (11), T_r is plotted in Fig. 3. Accompanying this plot is an approximation to Eq. (15) for $\Lambda \simeq I$ and $(I-J)(I-K) - P^2 \simeq [I-(J+K)/2]^2$, i.e., $T_r \simeq |\mathbf{H}/I|^2P^2(K-J) \times \sin\alpha\cos\alpha/[I-(J+K)/2]^2$. For the present system, this approximation is quite accurate. For the selected system parameters, direct egress from the minimum energy state is impossible since Fig. 3 indicates that a motor torque of 15 ft-lb is required while the net available torque [from Eqs. (11)] is only 1.25 ft-lb.

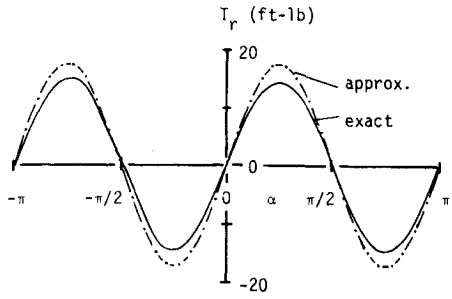

Fig. 3 Restraint torque as a function of α.

Excaping the Minimum Energy Trap

The hills and valleys in Fig. 2 suggest that a spacecraft with an undersized motor can escape its trap by pulsing the motor in a manner that induces growing oscillation of B relative to A about X_1, thereby gradually increasing kinetic energy. For this, an appropriate pulsing frequency must be selected, clearly one of the system's natural frequencies. These can be established by linearizing the equations of motion about the motion in the minimum energy state.

Noting that the trap state occurs for $\Omega = \alpha = 0$, the eigenvector of $[I]$ corresponding to $\Lambda(0)$ is found to lie in the X_1–X_3 plane. Since this eigenvector is the centroidal principal axis of maximum inertia of the system in the minimum energy state, and since the only stable motion of a quasi-rigid system must be spin about this axis, the minimum energy motion must be described by

$$[Z]^T = [\omega_{10}, 0, \omega_{30}, 0, 0] \tag{16}$$

where ω_{10} and ω_{30} are constants. Substitution of Eq. (16) into Eq. (2) with $T_1 = 0$ yields the condition

$$\omega_{10}\omega_{30}(I-K)+(\omega_{30}{}^2-\omega_{10}{}^2)P = 0 \tag{17}$$

A second constraint on ω_{10} and ω_{30} is produced by conservation of momentum [i.e., from Eqs. (10) and (16)]

$$|\mathbf{H}|^2 = (I\omega_{10}+P\omega_{30})^2+(K\omega_{30}+P\omega_{10})^2 \tag{18}$$

Equations (17) and (18) possess two solutions and, by evaluating K_e for each, the minimum energy state is found [for the parameters in Eqs. (11)] when

$$\omega_{30}/\omega_{10} = \left\{\left[\left(\frac{I-K}{P}\right)^2+4\right]^{1/2}-\left(\frac{I-K}{P}\right)\right\}\Big/2 \tag{19}$$

i.e., $\omega_{10} = 4.92$ rad/sec and $\omega_{30} = 1.23$ rad/sec.

Equation (2) may now be linearized about Eq. (16). Letting variables with asterisks denote the first-order perturbations of their counterparts, the resulting equations are

$$[E(0)][\dot{Z}^*]+[Q][Z^*] = [0, 0, 0, T_1, 0]^T \tag{20}$$

where [E(0)] is $[E]$ of Eq. (5) for $\alpha = 0$ and $[Q]$ is also a 5×5 matrix whose nonzero elements are as follows:

$$\begin{aligned}
Q_{12} &= P\omega_{10}+(K-J)\omega_{30} & Q_{15} &= P\omega_{30}\omega_{10}\\
Q_{21} &= (I-K)\omega_{30}-2P\omega_{10} & Q_{35} &= -P\omega_{10}{}^2\\
Q_{23} &= 2P\omega_{30}+(I-K)\omega_{10} & Q_{42} &= P\omega_{10}\\
Q_{24} &= B_1\omega_{30}-2P\omega_{10} & Q_{45} &= P\omega_{30}\omega_{10}\\
Q_{32} &= (J-I)\omega_{10}-P\omega_{30} & Q_{54} &= -1
\end{aligned} \tag{21}$$

System natural frequencies follow from the nonzero eigenvalues of $-[E(0)]^{-1}[Q]$, namely the roots of the characteristic polynominal

$$s(b_4s^4+b_2s^2+b_0) = 0 \tag{22}$$

where

$$\begin{aligned}
b_4 &= (I-B_1)J(P^2-B_1K)\\
b_2 &= \omega_{30}{}^2\{(J-K)(B_1K-P^2)(K-I+B_1)\}+\\
&\quad \omega_{10}{}^2\{(I-B_1)[(I-J)B_1(K-I)+P^2(J-K-B_1-3I)]\}+\\
&\quad \omega_{10}\omega_{30}\{(I-B_1)P[K(B_1-J)-B_1(I-J)-4P^2]\}\\
b_0 &= (J-K)P\omega_{10}\omega_{30}[2P^2(\omega_{10}{}^2+\omega_{30}{}^2)+\\
&\quad 2P(K+I)\omega_{10}\omega_{30}+(K-I)(K\omega_{30}{}^2-I\omega_{10}{}^2)]
\end{aligned} \tag{23}$$

For the system of Eqs. (11), these frequencies are $s_1 = 2.81$ rad/sec and $s_2 = 0.545$ rad/sec.

Frequency s_1 resembles the classical nutation frequency of a single rigid body. However, s_2 is a lower, and heretofore unidentified, frequency. The latter is often masked by symmetry assumptions since, when $J = K$, coefficient b_0 vanishes. The polynomial of Eq. (22) then has three zero roots and only one set of imaginary conjugates leading to a single eigenfrequency (the classical rigid body nutation frequency) whose magnitude is $|b_2/b_4|^{1/2}$.

Of the two possible excitation frequencies, that one offering greatest potential for escaping the trap may be determined by examining corresponding modes of free vibration about the energy trap solution. These follow from the eigenvectors of $-[E(0)]^{-1}[Q]$. For the parameters of Eqs. (11), the free vibrations of each mode are given by

$$\begin{bmatrix}\omega_1{}^*\\ \omega_2{}^*\\ \omega_3{}^*\\ \Omega^*\\ \alpha^*\end{bmatrix} = \begin{bmatrix}0\\ 0.0994\\ 0\\ 0\\ -5.26\end{bmatrix}\cos 0.545t + \begin{bmatrix}-0.0187\\ 0\\ 0.0438\\ 0.05\\ 0\end{bmatrix}\sin 0.545t \tag{24}$$

$$\begin{bmatrix}\omega_1{}^*\\ \omega_2{}^*\\ \omega_3{}^*\\ \Omega^*\\ \alpha^*\end{bmatrix} = \begin{bmatrix}0\\ 0.0309\\ 0\\ 0\\ 1.019\end{bmatrix}\cos 2.81t + \begin{bmatrix}-0.00113\\ 0\\ 0.0355\\ -0.05\\ 0\end{bmatrix}\sin 2.81t$$

where the first four entries in each column have units of rad/sec, the last entry has units of degrees, and the modes have been normalized to $|\Omega^*|_{max} = 0.05$ rad/sec. While normalization is such that Ω^* and $\omega_3{}^*$ are of comparable magnitude in either mode, the magnitude of α in the lower frequency mode is much greater than in the higher, suggesting that excitation at the former frequency will lead more efficiently to high amplitudes of α.

As a further check, one can use Eqs. (20) to compute the system frequency response in terms of peak α displacement per unit motor torque as shown in Fig. 4. The response at very low frequency is only 2°, indicating that statically the motor is incapable of providing the 90° relative rotation required for escape. The response is infinite at either natural frequency, but shows greater sensitivity in the neighborhood of the lower, suggesting that the system will be easier to excite there.

In practice, constant frequency excitation cannot lead to escape because the assumptions of linearity are invalid at large values of α. This problem can be circumvented by utilizing closed-loop

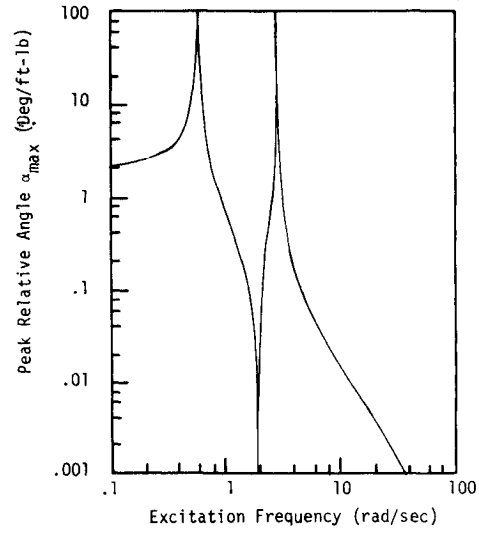

Fig. 4 Peak α response as a function of frequency.

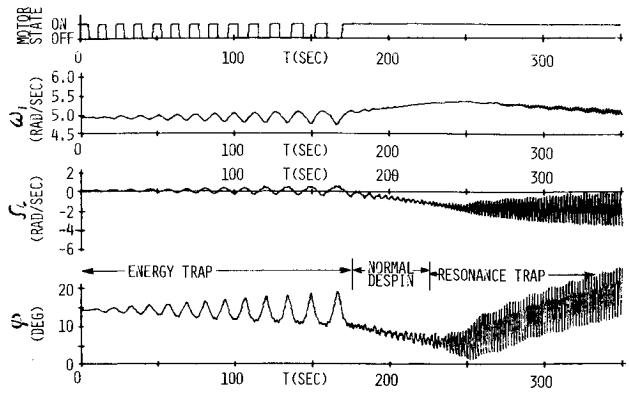

Fig. 5 Escaping the minimum energy trap and encountering resonance.

control of the motor to seek the varying excitation frequency. For the system of Eqs. (11), the motor torque is assumed unidirectional, applying to B only a negative torque about X_1 (tending to despin the platform). An appropriate law is to activate the motor for $\Omega \leqq 0$ and deactivate it for $\Omega > 0$. In the latter phase, friction removes energy, and increases in the amplitude of α can be achieved only if the net motor torque magnitude is more than double that of friction.

Implementation of this control law in a computer simulation of Eqs. (2) does lead to successful escape from the minimum energy trap. Time histories of the motor state, and of ω_1, Ω, and ϕ are shown in Fig. 5. Restricting attention to times less than 225 sec, and examining first the history of the motor state, a gradual lengthening in excitation period can be noted as the system departs from its linearized representation. After 170 sec, the relative rate Ω stays negative and the motor remains energized. The rotor spin rate ω_1 oscillates about its initial value of 4.92 rad/sec until the system escapes from the energy trap and then increases in a roughly linear fashion. Similarly, Ω oscillates about zero with ever increasing amplitude until escape is achieved and then proceeds toward its final goal of -6 rad/sec. Finally, the nutation angle ϕ oscillates about its initial value of 14° until the escape ($t = 179$ sec) and then begins a nearly linear descent. Thus using the motor to stimulate the system at the lower eigenfrequency, while lengthening the period as amplitudes grow, can indeed produce an escape from the minimum energy trap.

Resonance Trap

Nature of the Resonance Trap

The simulation results of Fig. 5 reveal an abrupt change in behavior part-way through the process of despinning the platform, i.e., at $t = 240$ sec. Specifically, while the motor remains activated, ω_1 ceases its growth and begins to decline. Simultaneously, Ω ceases its steady decline, maintaining a mean value of -1.5 rad/sec while oscillations about the mean grow more severe. Nutation no longer decays, but grows steeply both in mean value and in oscillations about the mean. This motion grows ever more violent as the motor adds energy to the system.

This phenomenon, hereafter called the resonance trap, is the second type of trap associated with the model in Fig. 1. The resonance and minimum energy traps appear to differ markedly. Specifically, the energy trap is characterized by simple spin, the lowest attainable kinetic energy, and constancy of $[Z]$. The resonance trap, by contrast, is one of violent motion, ever increasing energy (as long as the motor is activated), and oscillating elements in the state vector.

Consider first those conditions which produce the onset of resonance. It is hypothesized that, for the present system, resonance occurs whenever 1) the rotor's nutation frequency equals $|\Omega|$ or, equivalently, 2) the platform's nutation frequency equals $|2\Omega|$. The term "nutation frequency" has been used loosely here to mean the frequency analogous to that possessed by a completely balanced and symmetric dual-spin spacecraft. Indeed an analytical determination of frequencies for the present system has been achieved only near the minimum energy state where constant coefficient linear equations of motion can be assumed. By ignoring the effects of the platform dynamic imbalance and defining a mean transverse centroidal moment of inertia as $J^* = 0.5(J+K)$, approximate rotor and platform nutation frequencies, f_A and f_B, can be defined as

$$f_A = \omega_1(I/J^* - 1) + (B_1/J^*)\Omega$$
$$f_B = \omega_1(I/J^* - 1) + (B_1/J^* - 1)\Omega \tag{25}$$

Further, considering only small ϕ, the relationship between ω_1 and Ω for the hypothetical symmetric spacecraft can be approximated from Eqs. (10) as

$$|\mathbf{H}| \simeq h_1 \simeq I\omega_1 + B_1\Omega \simeq (I - B_1)\Omega_0 \tag{26}$$

where Ω_0 is the spin rate of A when B is despun and $\phi = 0$. Using Eqs. (25) and (26)

$$f_A = (1 - B_1/I)(I/J^* - 1)\Omega_0 + B_1\Omega/I$$
$$f_B = (1 - B_1/I)(I/J^* - 1)\Omega_0 + (B_1/I - 1)\Omega \tag{27}$$

The hypothesis, then, is that resonance occurs whenever

$$f_A = |\Omega| \quad \text{or} \quad f_B = |2\Omega| \tag{28}$$

Direct substitution from Eqs. (27) into either condition, taking $|\Omega| = -\Omega$ for $\Omega < 0$, provides

$$\Omega = \Omega_0(I/J^* - 1)(B_1/I - 1)/(B_1/I + 1) \tag{29}$$

For the parameters of the present system, Eq. (29) leads to $\Omega = -1.5$ rad/sec.

A heuristic justification for the hypothesis of Eqs. (28) can be made by regarding the nutation frequency of a spinning body as analogous to the natural frequency of a mass-spring system. It then follows that excitation of the body at this frequency will lead to unbounded response. Here, excitation is presumed to arise from periodic mass property variations occurring on the adjoining body of the dual-spin system. As viewed from the rotor of the present model, the platform's inertia tensor oscillates with a frequency equal to the mean relative rate; or as viewed from the platform, the rotor's inertia tensor varies at twice the mean relative rate. These observations lead directly to Eqs. (28). The two criteria provide the same critical speed because both f_A, f_B and the two apparent excitation frequencies differ by Ω. Figure 6 displays f_A, f_B, $|\Omega|$, and $|2\Omega|$ as functions of Ω for the system of Eqs. (11) over the range $-6 \leqq \Omega \leqq 0$. The two intersections denoting resonance are seen to occur when $\Omega = -1.5$ rad/sec.

While motion in the resonance trap does not appear to resemble that in the minimum energy trap, there are certain similarities which have been demonstrated by simulation. First, the phenomenon is dependent on both the rotor asymmetry and the platform dynamic imbalance, with removal of either

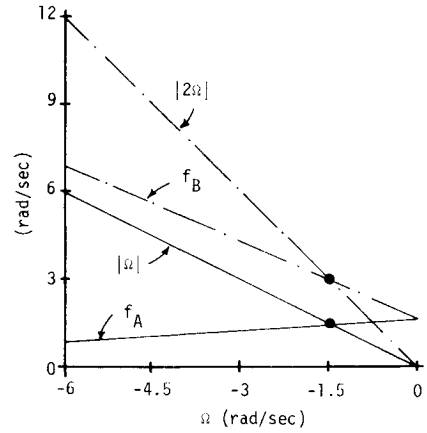

Fig. 6 Nutation frequencies as functions of relative rate.

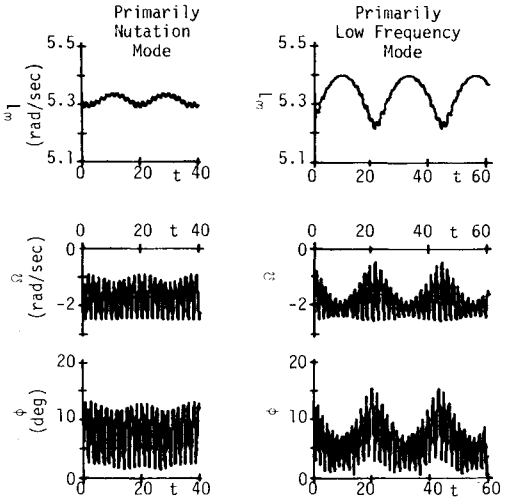

Fig. 7 Modes of free vibration in resonance.

condition eliminating the resonance. Second, the seriousness of the trap depends on motor torque magnitude; a sufficiently powerful motor will traverse the critical relative rate so rapidly that the trap is inconsequential. Third, and perhaps most significant, the system again exhibits two periodic modes of attitude motion, one mode corresponding roughly to classical nutation and the other having a markedly lower frequency and more pronounced excursions of ω_1 and Ω. Using computer simulation, one can demonstrate free vibrations (i.e., motions occurring with zero motor and friction torque) in which one or the other mode predominates while the system retains constant values of $|\mathbf{H}|$ and K_e. Time histories of ω_1, Ω, and ϕ illustrating this behavior for the system of Eqs. (11) appear in Fig. 7 for two cases where $K_e = 4698$ ft-lbs. The lower frequency mode (at approximately 0.28 rad/sec) manifests itself by modulating the envelope of the higher frequency (3.4 rad/sec) mode. The two cases show two different levels of low frequency modulation, one in which it is dominant and one in which it is not.

Escaping the Resonance Trap

This dual mode nature of resonance suggests the fourth similarity to the minimum energy trap, namely that excitation of the system by the motor at the appropriate frequency can lead to an escape from the resonance condition. This has been verified by simulation as shown in Fig. 8. Here time histories of the motor state, ω_1, Ω, and ϕ are shown starting with initial conditions corresponding to $t = 200$ sec in Fig. 5. The motion proceeds identically to that in Fig. 5 until $t = 252$ sec. at which time switching of the motor commences. Only two cycles of motor deactivation are required to alter the response, inducing the scalloping envelope characterizing the low frequency mode. The motor then remains energized until the intended relative rate of -6 rad/sec is attained ($t = 435$ sec). From that point, the motor torque alternates at a high frequency such that its mean value exactly cancels friction. Body B is now despun and A has attained its nominal speed. Some residual nutation remains; however, in an actual spacecraft with energy dissipation capability, this residual would decay to zero.

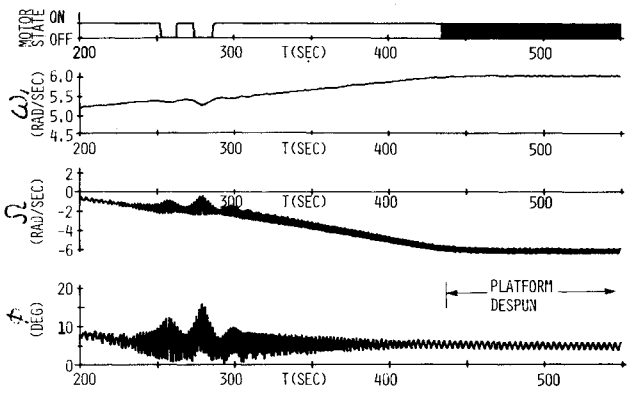

Fig. 8 Escaping the resonance trap and despinning the platform.

Thus, despite the apparent differences between the minimum energy and the resonance traps, there exist strong similarities. Unfortunately, the complexity of the equations of motion has frustrated attempts to analytically gain greater understanding of resonance. This remains a challenging problem for future research.

Conclusion

In summary, removal of the usual symmetry assumptions reveals two modes of attitude motion and two types of trap states for dual-spin spacecraft. One trap is characterized by minimum energy and benign motion, the other by increasing energy and violent motion. In either case, an undersized torque motor can stimulate the lower frequency mode, ultimately leading to escape. For future spacecraft design, these traps should be predicted and their effects subdued by either careful control of mass properties or selection of a sufficiently powerful motor.

References

[1] Flatley, T. W., "Equilibrium States for a Class of Dual-Spin Spacecraft," Ph.D. dissertation, 1970, Catholic University, Washington, D.C.

[2] Longman, R. W., "Stability Analysis of All Possible Equilibria for Gyrostat Satellites under Gravitational Torques," *AIAA Journal*, Vol. 10, No. 6, June 1972, pp. 800–806.

[3] Crespo da Silva, M. R. M., "Non-linear Resonant Attitude Motions in Gravity-Stabilized Gyrostat Satellites," *International Journal of Non-Linear Mechanics*, Vol. 7, 1972, pp. 621–641.

[4] Cloutier, G. J., "Stable Rotation States of Dual-Spin Spacecraft," *Journal of Spacecraft and Rockets*, Vol. 5, No. 4, April 1968, pp. 490–492.

[5] Sen, A. K., "On the Existence of a Trap State for OSO-Type Satellites," *IEEE Transactions on Automatic Control*, Vol. AC-17, No. 4, Aug. 1972, pp. 510–515.

[6] Likins, P. W., Tseng, G. T., and Mingori, D. L., "Stable Limit Cycles due to Nonlinear Damping in Dual-Spin Spacecraft," *Journal of Spacecraft and Rockets*, Vol. 8, No. 6, June 1971, pp. 568–574.

[7] Mingori, D. L., Tseng, G. T., and Likins, P. W., "Constant and Variable Amplitude Limit Cycles in Dual-Spin Spacecraft," *Journal of Spacecraft and Rockets*, Vol. 9, No. 11, Nov. 1972, pp. 825–830.

[8] McIntyre, J. E. and Gianelli, M. J., "Bearing Axis Wobble for a Dual Spin Vehicle," *Journal of Spacecraft and Rockets*, Vol. 8, No. 9, Sept. 1971, pp. 945–951.

[9] Wenglarz, R. A., "Dynamically Unbalanced Dual-Spin Space Stations with Rigid or Low-Coupling Interconnections," *Journal of Spacecraft and Rockets*, Vol. 8, No. 10, Oct. 1971, pp. 1032–1037.

[10] Cretcher, C. K. and Mingori, D. L., "Nutation Damping and Vibration Isolation in a Flexibly Coupled Dual-Spin Spacecraft," *Journal of Spacecraft and Rockets*, Vol. 8, No. 8, Aug. 1971, pp. 817–823.

[11] Sen, S. and Bainum, P. M., "The Motion and Stability of a Dual-Spin Satellite during the Momentum Wheel Spin-up Maneuver," *Journal of Spacecraft and Rockets*, Vol. 10, No. 12, Dec. 1973, pp.760–766.

[12] Barba, P. M., Furumoto, N., and Leliakov, I. P., "Techniques for Flat Spin Recovery of Spinning Satellites," AIAA Paper 73-859, Key Biscayne, Fla., 1973.

[13] Pringle, R. J., "On the Stability of a Body with Connected Moving Parts," *AIAA Journal*, Vol. 4, No. 8, Aug. 1966, pp. 1395–1404.